Ionics (2017) 23:1861–1869
DOI 10.1007/s11581-017-1986-0

ORIGINAL PAPER

Preparation of carbon-supported Pd-decorated PtCu nanoparticles towards formic acid oxidation reaction

Yange Suo[1] · Chenbin Rong[1] · Yuxin Guo[1] · Zhiguo Zhang[1] · Guilin Hu[1] · Yousheng Xu[1] · Xinfa Zhou[2]

Received: 21 September 2016 / Revised: 20 December 2016 / Accepted: 14 January 2017 / Published online: 22 January 2017

Abstract This work reports the synthesis of a novel carbon-supported Pd-decorated PtCu nanocatalyst for formic acid oxidation. Without using surfactants or polymers, PtCu alloy was firstly prepared through simply co-reduction of Pt and Cu ions using ethylene glycol and sodium citrate as the reducing and stabilizing reagents. Then, Pd was decorated on the surface of PtCu through spontaneous replacement of Cu by Pd. XRD results suggest that the lattice parameters of the PtCu and Pd-decorated PtCu nanoparticles are smaller than that of Pt. TEM images show that all metallic nanoparticles are well dispersed on the carbon surface. The average particle size of the Pd-decorated PtCu nanoparticles is 2.9 nm. Electrochemical analysis suggests that the carbon-supported Pd-decorated PtCu nanocatalyst exhibits an enhanced activity for formic acid oxidation in comparison with the carbon-supported Pt and carbon-supported PtCu, as well as a high stability in acidic medium.

Keywords PtCu · Pd · Formic acid oxidation · Fuel cell

Introduction

In recent years, direct formic acid fuel cell (DFAFC) has attracted lots of attentions due to its higher theoretical open circuit voltage and lower fuel crossover in comparison with the conventional direct methanol fuel cell (DMFC) [1]. Pd-based catalysts are found to be highly active towards formic acid oxidation [2–5]; however, the poor electrochemical stability of Pd greatly affects their practical applications [6]. Pt-based catalysts are another promising catalyst candidates for formic acid oxidation. It is widely accepted that formic acid oxidation on Pt follows the so-called dual-path mechanism [7]. The dehydrogenation pathway (direct pathway) involves the direct oxidation of HCOOH to CO_2, while the dehydration pathway (indirect pathway) involves the formation of poisonous species [8], which could block the active surface area of Pt and thus greatly affects its activity.

One strategy to enhance the catalytic activity of Pt is to modify Pt with another metal, such as Au [9–12], Mo [13], Bi [14], Ir [15], Pd [16], Ag [17], Pb [18], Sn [19], Cu [20–22], Au and Cu [23], to form alloy, core-shell, or inter-metallic structured materials. For instance, Pt-Cu alloys have been reported to exhibit higher activity towards formic acid oxidation compared with commercial Pt/C. The enhanced activity could be ascribed to the electronic effect generated through alloying Cu to Pt and the enhanced CO tolerance of PtCu alloy [24] or the synergetic effects between Pt and Cu [25]. Combining the advantages of Pt and Pd, PtPd bimetallic catalyst has also been found to exhibit high performance towards formic acid oxidation [26]. Baranova et al. [27] have prepared a series of PdPt/C catalysts with different metallic compositions through a modified polyol method using poly(*N*-vinyl-2-pyrrolidone) (PVP) as the stabilizing reagent. Electrochemical evaluation suggests that the PdPt/C catalysts exhibit much higher activity compared with Pt/C, as well as enhanced electrochemical stability in comparison with Pd/C. Except for bimetallic nanoparticles, the catalytic activity of trimetallic materials has also been

✉ Guilin Hu
enehgl@163.com

[1] Department of Energy and Environmental Systems Engineering, Zhejiang University of Science and Technology, Liuhe Road 318#, Hangzhou, Zhejiang Province 310023, China

[2] Zhejiang Institute of Energy and Nuclear Technology, Wener Road 218#, Hangzhou, Zhejiang Province 310012, China

explored. For instance, Jiang et al. [28] have reported the synthesis of PdPtCu trimetallic nanocatalysts for formic acid oxidation through co-reduction of Pd, Pt, and Cu ions.

In this work, in order to maximize the utilization of Pd and to take the advantages of both Pt and Pd, we have designed a novel carbon-supported Pd-decorated PtCu nanocatalyst for formic acid oxidation. Without using surfactants or polymers, PtCu alloy was firstly prepared through simply co-reduction of Pt and Cu ions using ethylene glycol and sodium citrate as the reducing and stabilizing reagents. Then, Pd was decorated on the surface of PtCu through spontaneous replacement of Cu by Pd. The physicochemical properties of the catalysts were characterized by X-ray diffraction (XRD), transmission electron microscopy (TEM), and X-ray photoelectron spectroscopy (XPS). Electrochemical analysis was carried out to evaluate the electrochemical properties of the catalysts.

Experimental

Chemicals

Chloroplatinic acid hexahydrate ($H_2PtCl_6{\cdot}6H_2O$), copper(II) sulfate pentahydrate ($CuSO_4{\cdot}5H_2O$), ethylene glycol ($C_2H_6O_2$), perchloric acid ($HClO_4$), sodium citrate ($C_6H_5Na_3O_7{\cdot}2H_2O$), and ethanol ($C_2H_5OH$) were purchased from Sinopharm Chemical Reagent Co., Ltd. Ammonium tetrachloropalladate ($(NH_4)_2PdCl_4$) and formic acid (HCOOH) were ordered from Aladdin. Vulcan XC-72 carbon was purchased from E-TEK. Nafion solution (5%) was received from Dupont.

Synthesis of the catalysts

All chemicals were of analytical grade and used as received. Carbon-supported PtCu catalyst (metallic loading of 20 wt%, atomic ratio of Pt to Cu being 3:1) was prepared using our previous developed method [29]. Firstly, 0.4349 g sodium citrate was dissolved into 80 ml water/ethylene glycol mixture solution (volume/volume = 1:1), and then 96 mg Vulcan XC-72 carbon was poured into the above solution to obtain the sodium citrate suspension, which was stirred and ultrasonically mixed for 2 h. At the same time, 5.7 ml chloroplatinic acid hexahydrate ($H_2PtCl_6{\cdot}6H_2O$) aqueous solution (1 g/100 ml) and 9.26 mg copper(II) sulfate pentahydrate ($CuSO_4{\cdot}5H_2O$) were dissolved into another 15 ml water/ethylene glycol solution (volume/volume = 1:1) to obtain the precursor solution. After removing air with N_2 bubbling for 30 min, the sodium citrate suspension was refluxed at 170 °C oil bath. After 15 min heating, the precursor solution was added into the heated sodium citrate suspension drop by drop. Another 55 ml water/ethylene glycol solution (volume/volume = 1:1) was added into the reaction system, which was then continued to be heated for another 2 h. The reaction product was filtered and washed with water and ethanol. The residue was dried at 60 °C for 12 h and then grounded in an agate mortar to get the carbon-supported PtCu nanoparticles (denoted as PtCu/C). Carbon-supported Pt nanoparticles (denotated as Pt/C) with Pt loading of 20 wt% and carbon-supported Pd nanoparticles (denotated as Pd/C) with Pd loading of 20 wt% were also prepared using the same protocol.

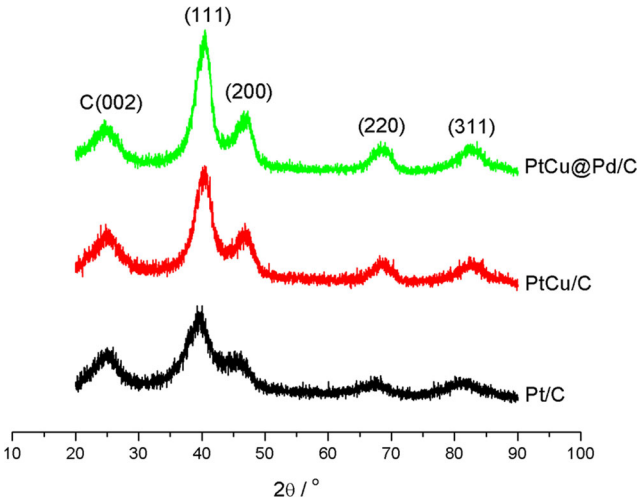

Fig. 1 XRD patterns of the *Pt/C*, *PtCu/C*, and *PtCu@Pd/C* catalysts

To decorate Pd on the surface of PtCu, a spontaneous replacement reaction was employed [30]. The standard redox potential of $PdCl_4^{2-}$/Pd (0.62 V vs. reversible hydrogen electrode (RHE)) is higher than that of Cu^{2+}/Cu (0.27 V vs. RHE) [31], spontaneous replacements of Cu with Pd could occur. The detailed procedures are as follows: 40 mg of the as-prepared PtCu/C was suspended in 20 ml ammonium tetrachloropalladate ($(NH_4)_2PdCl_4$) aqueous solution (containing 4.9 mg $(NH_4)_2PdCl_4$) and left stirred at room temperature for 12 h. The reaction product was filtered and dried to get the carbon-supported Pd-decorated PtCu catalyst (denotated as PtCu@Pd/C).

Physicochemical characterization

Powder XRD was carried out with an X-ray diffractometer (Ultima IV, Rigaku) using a Cu Kα radiation source. The values of diffraction angle and breadth of diffraction line at half-maximum intensity, obtained through fitting of (220) diffraction peak to a Lorentzian line shape, were used to calculate the crystalline size and lattice parameter. TEM was carried out with a JEM 2100 TEM system operated with LaB_6 filament at 200 kV. The average particle size was recorded through taking the size average of more than 200 particles. XPS was carried out with a PHI500 system. Inductively coupled plasma optical emission spectrometer (ICP-OES) was carried out with a VISTAMPXICP-720 system.

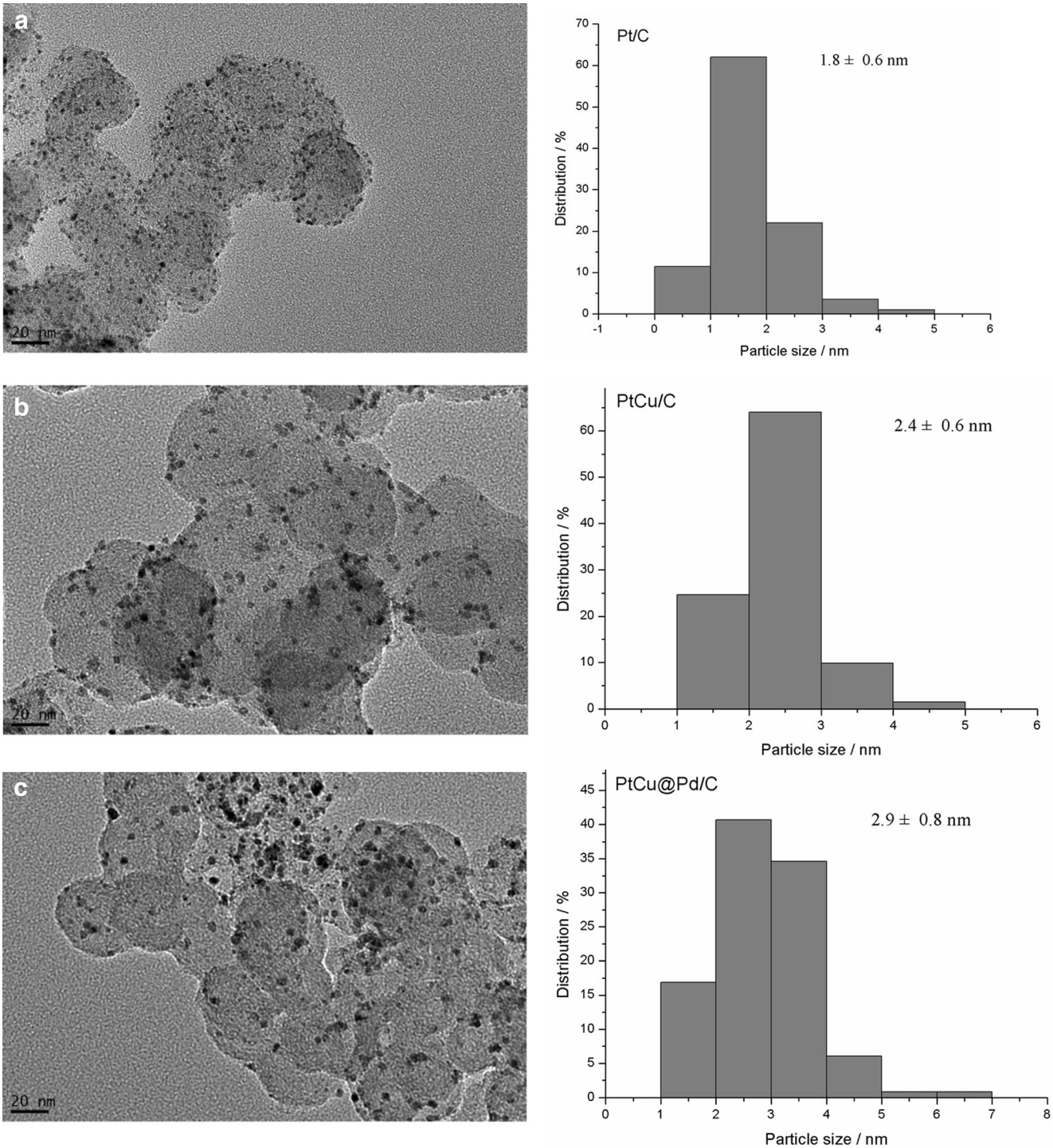

Fig. 2 TEM images of the **a** *Pt/C*, **b** *PtCu/C*, and **c** *PtCu@Pd/C* catalysts

Electrochemical evaluation

Electrochemical measurements were carried out using a CHI potentiostat (CHI600E). To do the electrochemical experiments, a conventional three-electrode cell, with a catalyst coated glassy carbon electrode (working electrode), a Pt coil (counter electrode), and a saturated Ag/AgCl electrode (reference electrode), was put into a 25 °C water tank. The glassy carbon substrate was polished with alumina suspension prior to use. To prepare the working electrode, 10 mg catalyst was dispersed ultrasonically in 2 ml diluted nafion solution (0.05 wt% in ethanol) for 30 min and 10 μl of the suspension was pipetted onto the glassy carbon electrode ($\phi = 5$ mm) by a microsyringe and left to dry at room temperature. Prior to the

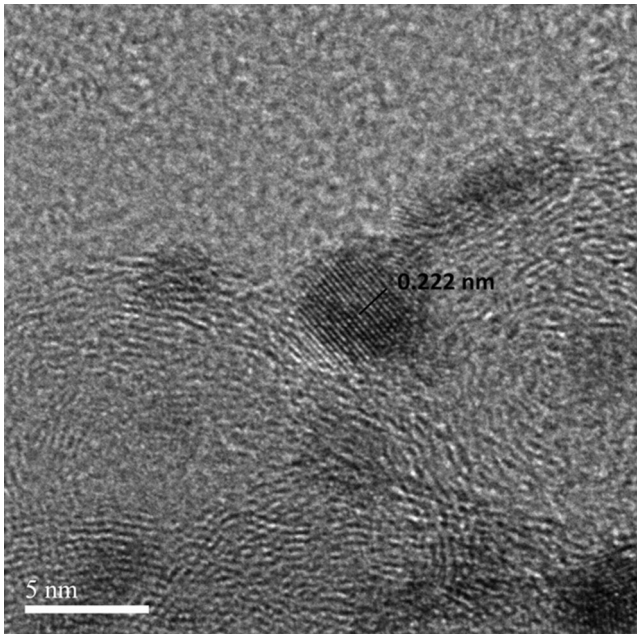

Fig. 3 HRTEM image of the PtCu@Pd/C catalyst

activity measurement, the working electrode was cleaned by cyclic voltammogram (CV) sweeping in N_2-saturated 0.5 M $HClO_4$ solution. Then, certain amount (in order to keep the concentration in the electrolyte as 0.5 M) of formic acid was added into the electrolyte to do the activity measurements.

Results and discussion

Structure and morphology characterization

XRD patterns of the Pt/C, PtCu/C, and PtCu@Pd/C catalysts are shown in Fig. 1. The broad diffraction peak at about 25° is ascribed to the (002) plane of Vulcan XC-72 carbon. All of the three catalysts exhibit characteristic diffraction peaks of face centered cubic (fcc) crystalline structure. Positions of the diffraction peaks of Pt/C catalyst fit well with the standard values of Pt. The corresponding diffraction peaks of PtCu/C catalyst exhibits a shift towards higher diffraction angles in comparison with Pt/C. The lattice parameter of PtCu/C catalyst calculated based on Bragg's law [32] using (220) diffraction peak is 3.874 Å, which is smaller than that of Pt/C (3.950 Å), indicating the formation of PtCu alloy. The alloying degree (detonated as the content of Cu in the Pt-Cu crystal) of the PtCu/C calculated based on the lattice parameter data is 23%, which is consistent with the stoichiometric content of Cu in the PtCu/C catalyst (i.e., 25%). This result suggests that Cu can be fully incorporated into the Pt lattice. The lattice parameter of the PtCu@Pd/C is 3.878 Å, similar with that of PtCu/C (3.874 Å). The average crystal size of the Pt/C, PtCu/C, and PtCu@Pd/C calculated based on Scherrer equation is 1.7, 2.8, and 2.7 nm, respectively, indicating that incorporation of Pd to PtCu does not induce the change of the average crystal size.

Fig. 4 **a** XPS spectra of the *Pt/C*, *PtCu/C*, and *PtCu@Pd/C* catalysts. **b** *Pt 4f* of the Pt/C catalyst. **c** *Pt 4f* of the PtCu/C catalyst. **d** *Pt 4f* of the PtCu@Pd/C catalyst. **e** *Cu 2p* of the PtCu/C catalyst. **f** *Cu 2p* of the PtCu@Pd/C catalyst. **g** *Pd 3d* of the PtCu@Pd/C catalyst

TEM images of the Pt/C, PtCu/C, and PtCu@Pd/C catalysts are shown in Fig. 2. It can be seen that the nanoparticles in the three catalysts are well dispersed on the carbon surface. The histogram of particle size distribution of each catalyst was obtained by recording more than 200 nanoparticles at different areas. The average particle sizes of Pt/C, PtCu/C, and PtCu@Pd/C are 1.8, 2.4, and 2.9 nm, respectively. The average particle sizes of the catalysts based on TEM characterization are well consistent with the values based on XRD characterization, which further confirms that there is little particle aggregation. Figure 3 shows the high-resolution TEM (HRTEM) image of the PtCu@Pd/C catalyst. An interplaner distance of 0.222 nm can be measured. The value is consistent with that of PtCu@Pd/C (111) crystallographic plane (0.224 nm) based on XRD measurement.

XPS characterization was performed to obtain surface information. Figure 4a shows the XPS spectra of the Pt/C, PtCu/C, and PtCu@Pd/C catalysts. Pt 4f spectra can be clearly seen on the three catalysts. However, no obvious Cu 2p or Pd 3d spectra are observed on the PtCu/C or PtCu@Pd/C catalysts, suggesting relatively low contents of Cu or Pd. Figure 4b–d shows the regional Pt 4f spectra of the Pt/C, PtCu/C, and PtCu@Pd/C catalysts. The Pt 4f exhibits a doublet including a low-energy band (Pt $4f_{7/2}$) and a high-energy band (Pt $4f_{5/2}$). The chemical states of Pt can be obtained through fitting the spectra to three pairs of overlapping curves, labeled as 1, 2, and 3, which can be ascribed to be Pt(0) chemical state, Pt(II) chemical state, and Pt(IV) chemical state, respectively [17]. The binding energies and relative intensities of the Pt 4f of the three catalysts are shown in Table 1. It can be seen that the relative intensity of Pt(0) in the PtCu@Pd/C catalyst is larger than that in the PtCu/C catalyst or Pt/C catalyst. Figure 4e, f shows the regional Cu 2p of the PtCu/C and PtCu@Pd/C catalysts. Similar to Pt 4f, Cu 2p also shows a doublet containing a low-energy band (Cu $2p_{3/2}$) and a high-energy band (Cu $2p_{1/2}$). The chemical states of Cu can be obtained through fitting the spectra to two pairs of overlapping curves, labeled as 1 and 2 which are ascribed to be Cu(0) chemical state and Cu(II) chemical state, respectively [33]. The binding energies and relative intensities of the Cu 2p of the two catalysts are presented in Table 1. Compared with that of PtCu/C, the intensity ratio of Cu(II) to Cu(0) in the PtCu@Pd/C catalyst is much larger, suggesting that there could be electron transfer from Cu to Pd or Pt through incorporation of Pd. The Pd 3d spectrum of the PtCu@Pd/C catalyst is shown in Fig. 4g. The peak at low-energy band is from

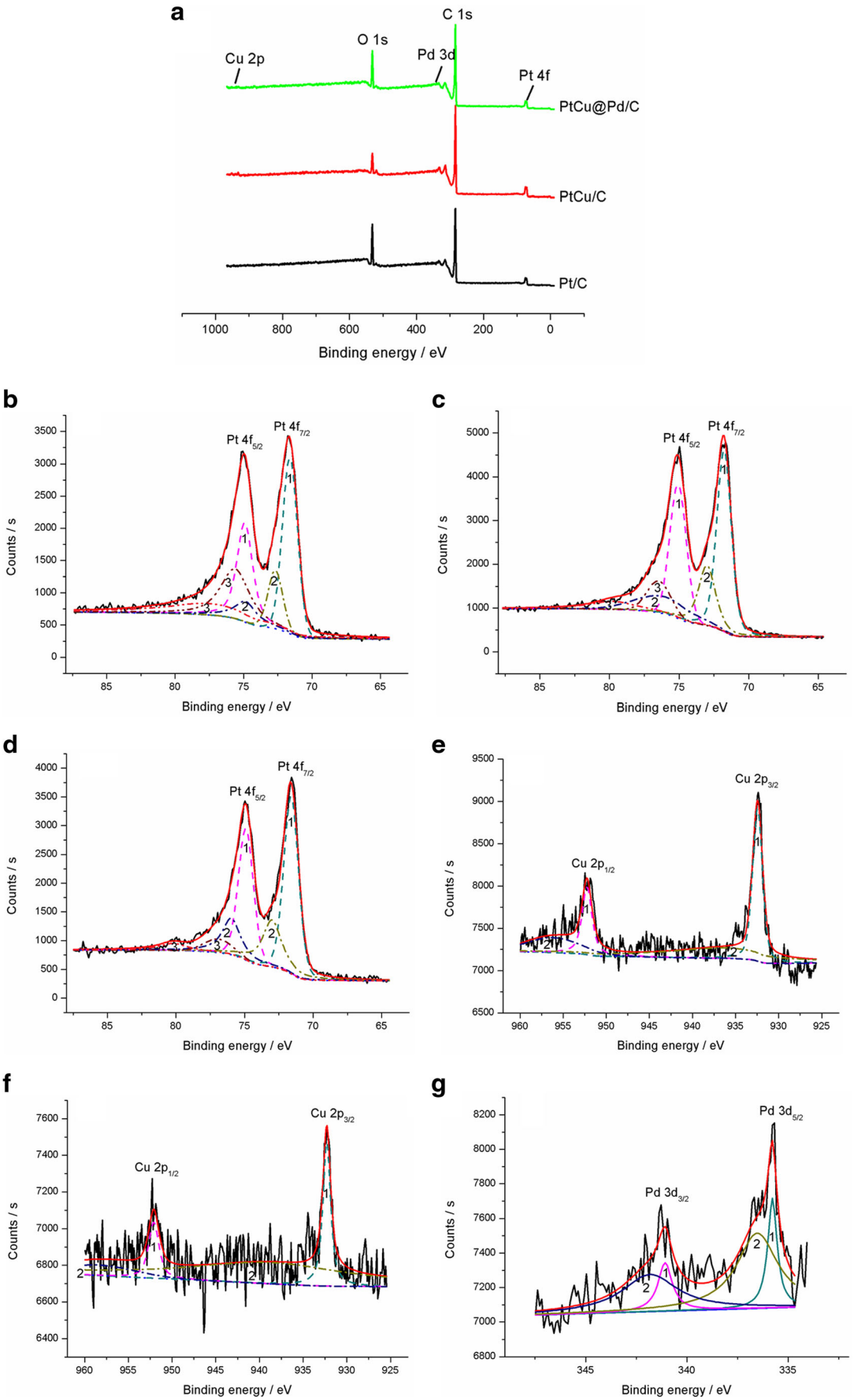
a
C 1s
O 1s
Cu 2p
Pd 3d
Pt 4f
PtCu@Pd/C
PtCu/C
Pt/C
Binding energy / eV
b
Pt 4f5/2
Pt 4f7/2
Counts / s
Binding energy / eV
c
Pt 4f5/2
Pt 4f7/2
Counts / s
Binding energy / eV
d
Pt 4f5/2
Pt 4f7/2
Counts / s
Binding energy / eV
e
Cu 2p3/2
Cu 2p1/2
Counts / s
Binding energy / eV
f
Cu 2p3/2
Cu 2p1/2
Counts / s
Binding energy / eV
g
Pd 3d5/2
Pd 3d3/2
Counts / s
Binding energy / eV

Table 1 Binding energies and relative intensities of different chemical states of Pt, Cu, and Pd in the Pt/C, PtCu/C, and PtCu@Pd/C catalysts

Sample	Species	Binding energy (eV)	Relative intensity (%)
Pt/C	Pt(0)	71.6	49
	Pt(II)	72.7	16
	Pt(IV)	75.6	35
PtCu/C	Pt(0)	71.8	59
	Pt(II)	73	26
	Pt(IV)	76.5	15
PtCu@Pd/C	Pt(0)	71.6	62
	Pt(II)	73	29
	Pt(IV)	76.9	9
PtCu/C	Cu(0)	932.4	52
	Cu(II)	936.3	48
PtCu@Pd/C	Cu(0)	932.3	22
	Cu(II)	938.6	78
PtCu@Pd/C	Pd(0)	335.8	25
	Pd(II)	336.5	75

Pd $3d_{5/2}$, and the peak at high-energy band is from Pd $3d_{3/2}$. As shown in Table 1, the relative intensity of Pd(II) is 75%, which is higher than that of Pd(0), indicating that Pd exists mainly in the oxidation state. Furthermore, from the XPS intensities, the surface atomic ratio of Pt to Cu in PtCu/C can be calculated to be 47: 53, which is lower than the stoichiometric value (75: 25), indicating enrichment of Cu element on the surface of the nanoparticles. The atomic ratio of Pt to Cu to Pd in the PtCu@Pd/C is 46:40:14, suggesting the replacement of Cu with Pd.

ICP-OES was carried out to determine the real metallic loadings of the catalysts. The real Pt loading in the Pt/C catalyst is 13.56 wt%. The loadings of Pt and Cu in the PtCu/C catalyst are 12.60 and 1.05 wt%, respectively. The loadings of Pt, Cu, and Pd in the PtCu@Pd/C catalyst are 12, 0.95, and 0.88 wt%, respectively.

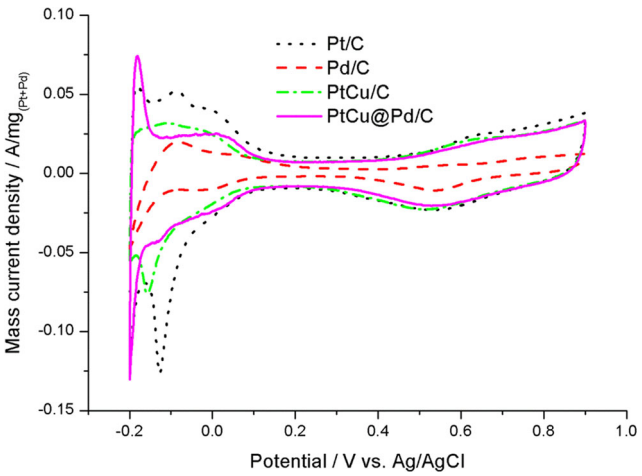

Fig. 5 Cyclic voltammograms of the *Pt/C*, *Pd/C*, *PtCu/C*, and *PtCu@Pd/C* catalysts in N_2-saturated 0.5 M $HClO_4$ solution at 25 °C with scan rate of 50 mV/s

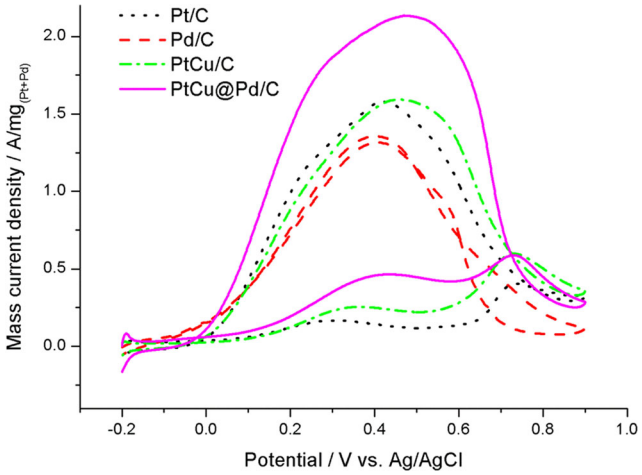

Fig. 6 Cyclic voltammograms of the *Pt/C*, *Pd/C*, *PtCu/C*, and *PtCu@Pd/C* catalysts in N_2-saturated 0.5 M HCOOH + 0.5 M $HClO_4$ at 25 °C with scan rate of 50 mV/s

Electrochemical characterization

Figure 5 shows the cyclic voltammograms of the Pt/C, Pd/C, PtCu/C, and PtCu@Pd/C catalysts in N_2-saturated $HClO_4$ solution. The obvious hydrogen desorption/adsorption current peaks at low potential range (i.e., −0.2–0.1 V) and surface oxidation/reduction at high potential range (i.e., higher than 0.3 V) are observed on the three Pt-based catalysts, which match with the typical CV characteristics of a "platinum-like" catalyst. Typical CV feature of palladium can be observed on the Pd/C catalyst.

Figure 6 shows the polarization curves of formic acid oxidation on the Pt/C, Pd/C, PtCu/C, and PtCu@Pd/C catalysts. The oxidation currents were normalized to the mass of Pt and Pd on the glassy carbon electrode. It can be seen that formic

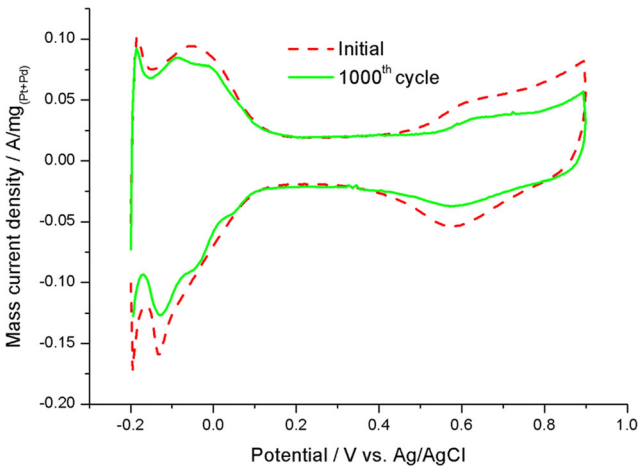

Fig. 7 Cyclic voltammograms (initial scan and 1000th cycle) of PtCu@Pd/C catalysts in N_2-saturated 0.5 M $HClO_4$ solution at 25 °C with scan rate of 100 mV/s

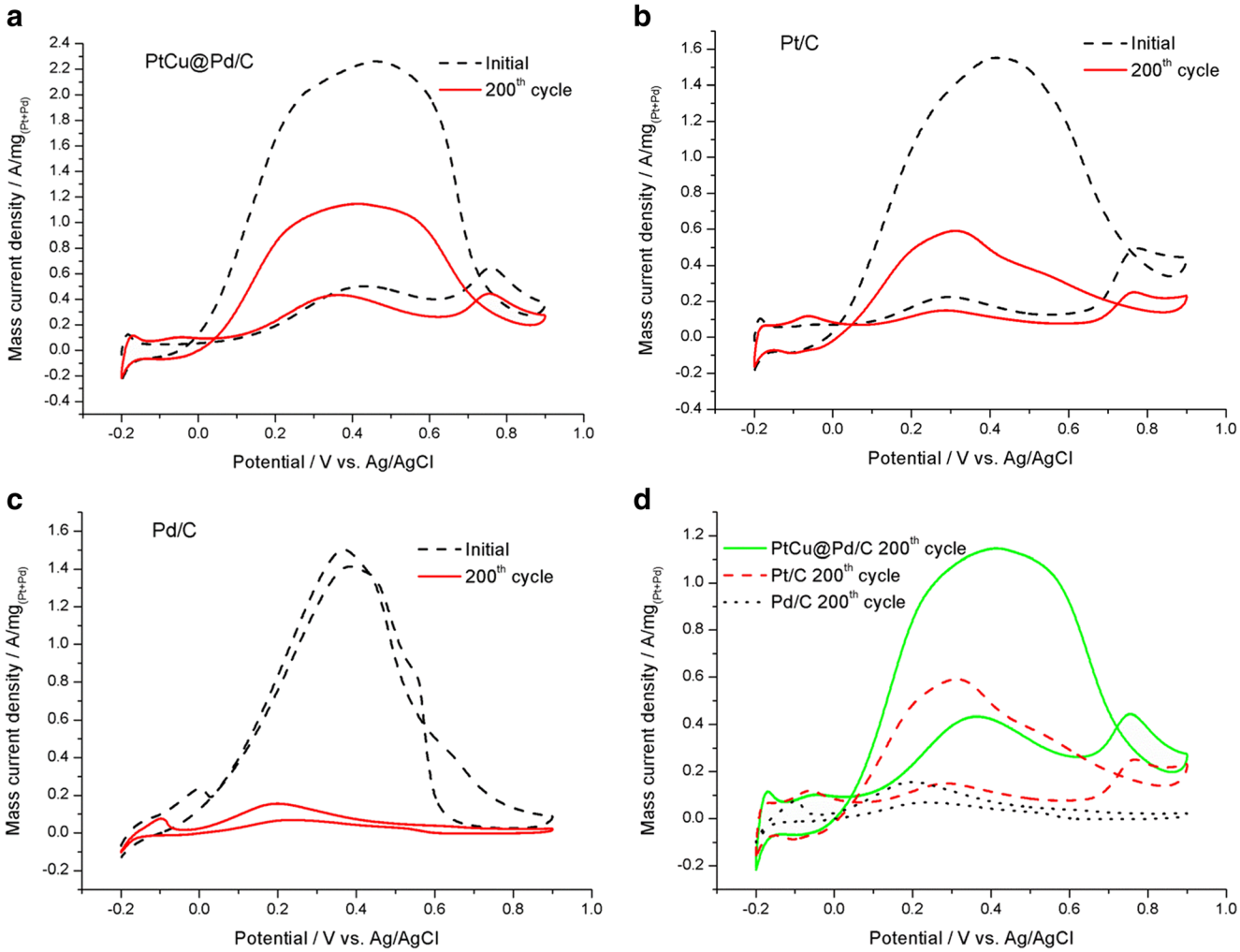

Fig. 8 Cyclic voltammograms (initial scan and 200th cycle) of **a** *PtCu@Pd/C*, **b** *Pt/C*, and **c** *Pd/C* catalysts in N_2-saturated 0.5 M HCOOH + 0.5 M $HClO_4$ at 25 °C with scan rate of 100 mV/s. **d** Comparison of the 200th cycle of *PtCu@Pd/C*, *Pt/C*, and *Pd/C* catalysts

acid oxidation on Pt/C exhibits two anodic peaks in the forward scan and one anodic peak in the backward scan. It is well known that formic acid oxidation on Pt undergoes dual pathway, i.e., a dehydrogenation pathway to form CO_2 directly and a dehydration pathway to generate adsorbed intermediate species (CO_{ads}), which block the active surface area of Pt, retarding the oxidation of formic acid. In the forward scan, the first anodic peak at about 0.3 V could be ascribed to the direct oxidation of formic acid on the remaining unblocked Pt surface, while the second oxidation peak at about 0.73 V is related to the oxidation of CO_{ads}. Oxidation of the poisonous CO_{ads} could release fresh Pt surface, resulting in the large oxidation current density in the backward scan. Similar cyclic voltammogram behavior can be observed on the PtCu/C catalyst. In comparison, the oxidation current density in the forward scan at high potential range (i.e., higher than 0.25 V) on PtCu/C is larger than that on Pt/C. Size-dependent activity of Pt towards formic acid oxidation has been widely studied. It is found that with the increase of particle size, the mass activity of Pt for formic acid oxidation decreases [34, 35]. Since the average particle size of PtCu alloy is larger than that of Pt in the current study, the observed larger oxidation current density of PtCu/C in the forward scan could not be induced by the particle size effect. The lattice strain effect has been found to induce a downshift of the d-band center [36]. The downshift of d-band center of PtCu in comparison with Pt results in a weaker interaction between CO and PtCu [37]. Therefore, easier removal of CO_{ads} could result in the increased current density of formic acid oxidation on PtCu/C than that on Pt/C in the forward scan. The oxidation current density on PtCu/C in the backward scan is similar with that on Pt/C. Moreover, the PtCu/C catalyst reported in this work exhibits a much higher mass activity compared with the previous work. The oxidation peak in the backward scan on our PtCu/C catalyst is about 1.6 times that on the previously reported PtCu/C catalyst [22]. Interestingly, when Cu is partially replaced by Pd, the formic acid oxidation current density increases a lot. Both the first oxidation peak in the forward scan and the oxidation

peak in the backward scan on PtCu@Pd/C are much larger than that on PtCu/C, indicating an enhanced dehydrogenation of formic acid on PtCu@Pd/C, which could be due to the synergistic effect between Pt and Pd [38]. The catalytic activity of Pd/C was also evaluated for comparison. It can be seen that, in terms of the forward scan, the oxidation current density on PtCu@Pd/C is much lower than that on Pd/C. Since formic acid oxidation on Pd mainly follows the dehydrogenation pathway with little CO_{ads} formation [39, 40], the blocking effect of CO_{ads} is not obvious on Pd, resulting in the much larger formic acid oxidation current density on Pd/C in the forward scan. However, the oxidation current density on PtCu@Pd/C in the backward scan is much higher than that on Pd/C.

Cyclic voltammetry was carried out to evaluate the stability of the PtCu@Pd/C catalyst. Figure 7 compares the CV of the initial cycle with that of the 1000th cycle in N_2-saturated $HClO_4$ solution. The electrochemical surface area (determined by the peak area of the surface oxide reduction at about 0.58 V) of the 1000th CV cycle has decreased to be 58% of its original value.

Figure 8 compares the stability of PtCu@Pd/C with that of Pt/C and Pd/C in N_2-saturated $HClO_4$ solution containing formic acid. From Fig. 8a–c, it can be seen that there is obvious current decay with potential cycling on the three catalysts. However, the current decay rate on PtCu@Pd/C is much lower than that on Pt/C or Pd/C. The peak current density of formic acid oxidation in the backward scan on PtCu@Pd/C decreases to be 51% of its initial value after 200 potential cycling. Comparatively, the peak current density of formic acid oxidation in the backward scan on Pt/C and Pd/C decreases to be 31 and 5% of initial value, respectively. The results suggest an enhanced electrochemical stability of PtCu@Pd/C compared with Pt/C or Pd/C. Figure 8d shows the 200th cycle of formic acid oxidation on PtCu@Pd/C, Pt/C, and Pd/C catalysts. Clearly, after 200th CV sweeping, the catalytic activity of PtCu@Pd/C is the highest among the three catalysts.

Conclusion

This work reports the synthesis of a novel carbon-supported Pd-decorated PtCu nanocatalyst for formic acid oxidation. Without using surfactants or polymers, PtCu alloy was firstly prepared through simply co-reduction of Pt and Cu ions using ethylene glycol and sodium citrate as the reducing and stabilizing reagents. Then, Pd was decorated on the surface of PtCu through spontaneous replacement of Cu by Pd. XRD results suggest that the lattice parameters of the PtCu- and Pd-decorated PtCu nanoparticles are smaller than that of Pt. TEM images show that all metallic nanoparticles are well dispersed on the carbon surface. The average particle size of the Pd-decorated PtCu nanoparticles is 2.9 nm. Electrochemical analysis suggests that the carbon Pd-decorated PtCu nanocatalyst exhibits an enhanced activity for formic acid oxidation in comparison with the carbon-supported Pt and carbon-supported PtCu, as well as a high stability in acidic medium.

Acknowledgements This work is financially supported by the Zhejiang Provincial Natural Science Foundation of China (LQ16B030001), the Project of Key Laboratory of Food Logistics Equipment and Technology of Zhejiang Province (KF2016016zd), the Project of Interdisciplinary Research in Zhejiang University of Science and Technology (2015JC02Y), and the Technical Plan Project of Zhejiang Province Science and Technology of China (2015F50023). We are thankful for the financial support of China Scholarship Council (201308330369).

References

1. Zhu Y, Ha SY, Masel RI (2004) High power density direct formic acid fuel cells. J Power Sources 130:8–14
2. Babu PK, Kim HS, Chung JH, Oldfield E, Wieckowski A (2004) Bonding and motional aspects of CO adsorbed on the surface of Pt nanoparticles decorated with Pd. J Phys Chem B 108:20228–20232
3. Liu Z, Hong L, Tham MP, Lim TH, Jiang H (2006) Nanostructured Pt/C and Pd/C catalysts for direct formic acid fuel cells. J Power Sources 161:831–835
4. Zhu F, Ma G, Bai Z, Hang R, Tang B, Zhang Z, Wang X (2013) High activity of carbon nanotubes supported binary and ternary Pd-based catalysts for methanol, ethanol and formic acid electro-oxidation. J Power Sources 242:610–620
5. Zhu F, He Y, Ma G, Zhang Z, Wang X (2014) A comparative study of elemental additives (Ni, Co and Ag) on electrocatalytic activity improvement of PdSn-based catalysts for ethanol and formic acid electro-oxidation. Electrochim Acta 148:291–301
6. Jung WS, Han J, Yoon SP, Nam SW, Lim T, Hong S (2011) Performance degradation of formic acid fuel cell incorporating a Pd anode catalyst. J Power Sources 196:4573–4578
7. Capon A, Parsons R (1973) Oxidation of formic acid at noble metal electrodes part III. Intermediates and mechanism on platinum electrodes. J Electroanal Chem 45:205–231
8. Beden B, Bewick A, Lamy C (1983) A study by electrochemically modulated infrared reflectance spectroscopy of the electrosorption of formic acid at a platinum electrode. J Electroanal Chem 148: 147–160
9. Xu J, Zhao T, Liang Z, Zhu L (2008) Facile preparation of AuPt alloy nanoparticles from organometallic complex precursor. Chem Mater 20:1688–1690
10. Kim Y, Kim HJ, Kim YS, Choi SM, Seo MH, Kim WB (2012) Shape- and composition-sensitive activity of Pt and PtAu catalysts for formic acid electrooxidation. J Phys Chem C 116:18093–18100
11. Oko DN, Zhang J, Garbarino S, Chaker M, Ma D, Tavares AC, Guay D (2014) Formic acid electro-oxidation at PtAu alloyed nanoparticles synthesized by pulsed laser ablation in liquids. J Power Sources 248:273–282
12. Xu J, Zhang C, Wang X, Ji H, Zhao C, Wang Y, Zhang Z (2011) Fabrication of bi-modal nanoporous bimetallic Pt-Au alloy with excellent electrocatalytic performance towards formic acid oxidation. Green Chem 13:1914–1922
13. Gojković SL, Tripković AV, Stevanović RM, Krstajić NV (2007) High activity of Pt_4Mo alloy for the electrochemical oxidation of formic acid. Langmuir 23:12760–12764

14. Zhang B-W, He C-L, Jiang Y-X, Chen M-H, Li Y-Y, Rao L, Sun S-G (2012) High activity of PtBi intermetallics supported on mesoporous carbon towards HCOOH electro-oxidation. Electrochem Commun 25:105–108
15. Chen W, Chen S (2011) Iridium-platinum alloy nanoparticles: composition-dependent electrocatalytic activity for formic acid oxidation. J Mater Chem 21:9169–9178
16. Lee J-Y, Kwak D-H, Lee Y-W, Lee S, Park K-W (2015) Synthesis of cubic PtPd alloy nanoparticles as anode electrocatalysts for methanol and formic acid oxidation reactions. Phys Chem Chem Phys 17:8624–8648
17. Xu J, Zhao T, Liang Z, Zhu L (2008) Synthesis of active platinum silver alloy electrocatalyst toward the formic acid oxidation reaction. J Phys Chem C 112:17362–17367
18. Huang Y, Zheng S, Lin X, Su L, Guo Y (2012) Microwave synthesis and electrochemical performance of a PtPb alloy catalyst for methanol and formic acid oxidation. Electrochim Acta 63:346–353
19. Habibi B, Delnavaz N (2012) Electrosynthesis, characterization and electrocatalytic properties of Pt-Sn/CCE towards oxidation of formic acid. RSC Adv 2:1609–1617
20. Ge X, Chen L, Kang J, Fujita T, Hirata A, Zhang W, Jiang J, Chen M (2013) A core-shell nanoporous Pt-Cu catalyst with tunable composition and high catalytic activity. Adv Funct Mater 23: 4156–4162
21. Qiu HJ, Xu HT, Li X, Wang JQ, Wang Y (2015) Core-shell-structured nanoporous PtCu with high Cu content and enhanced catalytic performance. J Mater Chem A 3:7939–7944
22. Huang Y, Zhao T, Zeng L, Tan P, Xu J (2016) A facile approach for preparation of highly dispersed platinum-copper/carbon nanocatalyst toward formic acid electro-oxidation. Electrochim Acta 190:956–963
23. Wang M, He Y, Li R, Ma Z, Zhang Z, Wang X (2015) Electrochemical activated PtAuCu alloy nanoparticle catalysts for formic acid, methanol and ethanol electro-oxidation. Electrochim Acta 176:259–269
24. Jiang Y, Jia Y, Zhang J, Zhang L, Huang H, Xie Z, Zheng L (2013) Underpotential deposition-induced synthesis of composition-tunable Pt-Cu nanocrystals and their catalytic properties. Chem Eur J 19:3119–3124
25. Chen S, Su H, Wang Y, Wu W, Zeng J (2014) Size-controlled synthesis of platinum-copper hierarchical trigonal bipyramid nanoframes. Angew Chem Int Ed 53:1–7
26. Li Z, Li M, Han M, Zeng J, Li Y, Guo Y (2014) Preparation and characterizations of highly dispersed carbon supported Pd_xPt_y/C catalysts by a modified citrate reduction method for formic acid electrooxidaiton. J Power Sources 254:183–189
27. Baranova EA, Miles N, Mercier PHJ, Page YL, Patarachao B (2010) Formic acid electro-oxidation on carbon supported Pd_xPt_{1-x}/C ($0 \geq x \geq 1$) nanoparticles synthesized via modified polyol method. Electrochim Acta 55:8182–8188
28. Jiang K, Cai W (2014) Carbon supported Pd-Pt-Cu nanocatalysts for formic acid electrooxidation: synthetic screening and componential functions. Appl Catal B Environ 147:185–192
29. Suo Y, Hsing I-M (2011) Synthesis of bimetallic PdAu nanoparticles for formic acid oxidation. Electrochim Acta 56:2174–2183
30. Wang D, Lin H, Wang H, Yu Y, Rus E, Muller DA, DiSalvo FJ, Abruña HD (2012) Facile synthesis of carbon supported Pd-Co core-shell nanoparticles as oxygen reduction electrocatalysts and their enhanced activity and stability with monolayer Pt decoration. Chem Mater 24:2274–2281
31. Antelman MS, Jr FJH (1982) The encyclopedia of chemical electrode. Potentials, Plenum Press, New York
32. Jenkins R, Snyder RL (1996) Introduction to X-ray powder diffractometry. Wiley, New York
33. Lu L, Shen L, Shi Y, Chen T, Jiang G, Ge C, Tang Y, Chen Y, Lu T (2012) New insights into enhanced electrocatalytic performance of carbon supported Pd-Cu catalyst for formic acid oxidation. Electrochim Acta 85:187–194
34. Rhee CK, Kim B-J, Ham C, Kim Y-J, Song K, Kwon K (2009) Size effect of Pt nanoparticle on catalytic activity in oxidation of methanol and formic acid: comparison to Pt(111), Pt(100) and polycrystalline Pt electrodes. Langmuir 25:7140–7147
35. Godinez-Salomón F, Arce-Estrada E, Hallen-López M (2012) Elelctrochemical study of the Pt nanoparticles size effect in the formic acid oxidation. Int J Electrochem Sci 7:2566–2576
36. Mavrikakis M, Hammer B, Nøskov JK (1998) Effect of strain on the reactivity of metal surfaces. Phys Rev Lett 81:2819–2822
37. Kang W, Li R, Wei D, Xu S, Wei S, Li H (2015) CTAB-reduced synthesis of urchin-like Pt-Cu alloy nanostructures and catalysis study towards the methanol oxidation reaction. RSC Adv 5: 94210–94215
38. Feng L, Si F, Yao S, Cai W, Xing W, Liu C (2011) Effect of deposition sequences on electrocatalytic properties of PtPd/C catalysts for formic acid electrooxidation. Catal Commun 12:772–775
39. Suo Y, Hsing I (2009) Size-controlled synthesis and impedance-based mechanistic understanding of Pd/C nanoparticles for formic acid oxidation. Electrochim Acta 55:210–217
40. Arenz M, Stamenkovia V, Schmidt TJ, Wandelt K, Ross PN, Markovia NM (2003) The electro-oxidation of formic acid on Pt-Pd single crystal bimetallic surfaces. Phys Chem Chem Phys 5: 4242–4251